Taphonomy of early life (2.1 Ga) in the francevillian basin (Gabon): Role of organic mineral interactions

Julie Ngwal'Ghoubou Ikouanga, Claude Fontaine, Franck Bourdelle, Ahmed Abd Elmola, Jérémie Aubineau, Olabode Bankole, Laurie Reisberg, Anne-Catherine Pierson-Wickmann, Armelle Riboulleau, Alain Trentesaux, et al.

Ms. Ref. No.: Ref.: Ms. No. PRECAM-D-23-00230

Taphonomy of early life (2.1 Ga) in the Francevillian Basin (Gabon): Role of organic mineral interactions

Julie Ngwal'ghoubou Ikouanga[a], Claude Fontaine[a], Franck Bourdelle[b], Ahmed Abd Elmola[a], Jérémie Aubineau[c], Olabode M. Bankole[a], Laurie Reisberg[d], Anne-Catherine Pierson-Wickmann[e], Armelle Riboulleau[f], Alain Trentesaux[f], Claude Laforest[a], Alain Meunier[a], Abderrazak El Albani [a]*

[a]University of Poitiers, UMR 7285 CNRS, IC2MP, F-86073, Poitiers Cedex 9, France.
[b]CY Cergy Paris Université, GEC Laboratoire Géosciences & Environnement Cergy, 95000 Neuville-sur-Oise, France
[c]Geosciences Montpellier, UMR 5243, CC 60 – University of Montpellier, F-34095 Montpellier, France
[d]Centre de Recherches Pétrographiques et Géochimiques, UMR 7358 CNRS - Université de Lorraine, F-54500, Vandoeuvre-lès-Nancy, France.
[e]University of Rennes, CNRS, Géosciences Rennes - UMR 6118, F-35000 Rennes, France.
[f]UMR 8187 LOG CNRS, University of Lille, ULCO, 59655 Villeneuve d'Ascq, France.

*Corresponding author.
E-mail address: abder.albani@univ-poitiers.fr (A. El Albani)

Abstract

The taphonomy of early soft-bodied organisms in Palaeoproterozoic sediments is not yet clearly understood, even though some locations where these fossils are found present all the conditions for exceptional fossil preservation. Indeed, the degree of fossil preservation has received attention, but better knowledge of the environmental conditions and associated taphonomic processes is also essential. In the Gabonese Francevillian Basin, the discovery of macrofossils (2.1 Ga) of multicellular organisms in black shales is an outstanding example of this degree of preservation. Indeed, the biological diversity, as a wide variety of fossil morphologies are observed, is associated with two major taphonomic processes – moulding (lenticular-shaped forms) or early pyritization, while the fossil host rocks were not deeply buried and were affected only by weak to moderate diagenesis. However, usually, the mechanisms of this preservation remain difficult to assess, as the original taphonomic processes are impacted by diagenesis and still misunderstood. In this way, by closely observing fossil mineralization in four morphotypes of macrofossils and associated host rocks from mineralogical and textural points of view, this work aims to provide some keys to a taphonomic comprehension of soft-bodied organism preservation. After the deposition of dead organisms on the clayey sediment, an illitization process, which depends on the availability of dissolved K driven by bacterial activity, started from the first stages of preservation by moulding the lenticular-shaped forms and proceeded in the pores of the other macrofossils after their pyritization. At the fossil level, the intensity of illitization is controlled by the mode of preservation and the evolution of the associated permeability. In the nonpyritized lenticular-shaped specimens, illitization was not achieved, preserving I-S mixed-layer minerals, while in the pyritized forms, the illitization degree was more extensive. In comparison, I-S mixed-layer minerals are almost absent in pyritized abiotic concretions. A second process, which occurred later, consists of general chloritization from fluid circulation. Our detailed results show that each specimen behaved like a microsystem with its own physico-chemical and mineralogical evolution during preservation/diagenesis. This finding allows us to propose a conceptual model of the taphonomic history, describing the fossilization stages for each type of specimen.

1. Introduction

Knowledge of early Precambrian biospheres is primarily based on the study of exceptionally well-preserved fossilized remains of soft-bodied organisms (Knoll, 1985). Shales appear to be very favourable host rocks for the preservation of the earliest forms of life (Ngombi-Pemba et al., 2014; Wilson and Butterfield, 2014), but the mechanisms of this preservation remain difficult to assess, as the original taphonomic processes are still largely misunderstood and can be impacted by various chemical and mineralogical transformations.

In fact, the preservation of soft bodies involves sufficiently slow biological degradation for the more resistant organic molecules to be fossilized by imprinting or mineralization (Briggs, 2003). The early stage of this preservation is mainly controlled by the nature of the sediments and their rate of accumulation (Briggs and Kear, 1993) in the presence or absence of biological agents (bacteria) together with the water column chemistry (major elements, dissolved O_2, etc.) of the depositional environment (Gaines et al., 2012; Gaines and Droser, 2010). Then, diagenetic processes (e.g., compaction, cementation, fluid–rock interaction, and potential hypothermal and magmatic activities) can also impact the quality of fossilization (Muscente et al., 2015). The quality of the conserved fossils, i.e., the degree of resemblance to the original organisms, is controlled by the intensity of all these predominant factors, with a direct impact on reconstructing the initial form of soft-bodied organisms and deriving information on their lifestyles based on the geometric (morphologies, tracks, burrows, etc.) and chemical (organic molecules, isotopes, etc.) signatures that have been preserved.

The Palaeoproterozoic fossil-rich black shales of the Francevillian Basin (Gabon) constitute a unique case study to fill these gaps. They hold exceptionally fossilized fauna, the oldest ecosystem is 2.1 billion years, they consist of decimetric macrofossils (El Albani et al., 2023, 2014, 2010; Ossa et al., 2023) of soft-bodied organisms capable of movement (El Albani et al., 2019a), and they are in close association with photosynthetic microbial mats (Aubineau et al., 2019, 2018; Reynaud et al., 2018). However, even if this fossiliferous system was not affected by metamorphic conditions – thereby saving a large amount of taphonomic information (El Albani et al., 2014, 2019a; Gauthier-Lafaye and Weber, 1989; Ngombi-Pemba et al., 2014; Ossa Ossa et al., 2013; Weber, 1968a) – the fossilization/preservation conditions and mechanisms are still unclear. An adapted mineralogical and petrographic study of these organic matter-/clay-rich rocks should remove these uncertainties.

In this way, by closely observing fossil mineralization and host rocks from mineralogical and textural points of view and by describing organo-mineral interactions, this work aims to provide some keys to a taphonomic comprehension of soft-bodied organism preservation in Francevillian black shales. The study strategy involves the following:

(i) Remains of both biomineralized and nonmineralized taxa in fossil deposits were discriminated (Conway Morris, 1986).

(ii) Pyritic concretions that have no apparent links with the fossil specimens were observed (El Albani et al., 2023, 2019b, 2014, 2010; Ossa et al., 2023). This can help us to better understand the conditions that prevailed during fossilization.

(iii) Organo-mineral interactions were characterized. This can serve as indirect evidence for understanding the taphonomy and biogenicity of the earliest organisms (Lepot, 2020), especially clay mineral transformation, which can record palaeobiological and palaeoecological variations (Behrensmeyer et al., 2000). In this sense, resolving the role of minerals in the fossilization of soft bodies is also a key element in understanding any environmental bias in fossil assemblages. Illustrating the importance of organo-mineral interactions, Burges Shales fossils are certainly preserved primarily as carbonaceous compressions (Butterfield, 1995), but diagenetic mineralization may have stabilized organic matter or replicated the morphology (Anderson et al., 2011; Briggs, 2003).

Although the mineralogical study of Palaeoproterozoic Francevillian rocks has already been carried out in part (e.g., Aubineau et al., 2021), a systematic study such as the one presented here is unprecedented. Clay minerals, specifically illite, mixed-layer minerals (MLMs) and chlorite, have been documented within or near the fossils but not on a large scale with as many samples as in this study (more than 40 fossils + host rock samples). In this respect, our approach is resolutely innovative: it systematically characterizes the mineralogy and textural arrangement of clay minerals and pyrite in the host rock as well as in the fossils but independently assesses nonpyritized lenticular-shaped specimens, pyritized lobate forms, string-shaped specimens, and segmented morphologies. The results should allow us to propose a conceptual model depicting the taphonomy and the mechanisms of mineralization during fossilization and diagenesis according to the submillimetre-scale physico-chemical conditions.

2. Geological settings

The Franceville Basin is filled by a series of unmetamorphosed sedimentary deposits of Palaeoproterozoic age resting unconformably on an Archean basement (Figs. 1 and 2) (Aubineau et al., 2021; Bankole et al., 2015; Bros et al., 1992; Gauthier-Lafaye, 1986; Ossa Ossa et al., 2013; Thiéblemont et al., 2014; Weber, 1968a). The Francevillian siliciclastic fluvial and marine sediments are subdivided into four major lithostratigraphic formations, FA to FD, from oldest to youngest. The FA Formation dominantly consists of fluvio-deltaic conglomerates and sandstones (Bankole et al., 2015; Gauthier-Lafaye and Weber, 1989), while the overlying FB Formation is dominated by heterolithic marine rocks deposited during a period of tectonic subsidence and basin deepening (Reynaud et al., 2018). The significant lithological differences and sedimentary structures within this formation resulted in several lithostratigraphic subdivisions into the FB_1 (including a, b, and c units) and FB_2 (a and b units) members (Azziley Azzibrouck, 1986; Weber, 1968b). The FC Formation hosts shallow marine dolostones and cyanobacteria-hosting stromatolitic cherts interbedded with black shale horizons (Lekele Baghekema et al., 2017; Préat et al., 2011), while the FD Formation is made of marine black shales with

interbedded volcanic tuffs, which were deposited in a transgressive phase (Thiéblemont et al., 2014). Although large-scale synclinals and anticlinals have been formed in the Francevillian subbasin, sediments were not deformed, which is marked by the exceptional conditions of preservation of the entire Francevillian sedimentary stratum.

The Francevillian fossil deposits, which belong to the FB_2 Member, are in the Moulendé quarry close to Franceville town on the northern side of the Mvengué syncline. The latter stretches along an NNW–SSE axis parallel to the edge of the basin represented by the eastern boundary of the Chaillu Massif (Fig. 1). The tectonic activity with the generation of normal faults predominantly in the centre of the Francevillian subbasin led to the formation of well-exposed outcrops (Fig. 2); (Gauthier-Lafaye and Weber, 1989; Mayaga-Mikolo, 1996; Thiéblemont et al., 2009; Weber, 1968b). Sea-level fall that began during the deposition of the FB_{1c} unit and extended during the deposition of the overlying FB_2 Formation caused contemporary-level to increasingly oxic conditions in the water column with transient oxygen-deficient bottom waters (Aubineau et al., 2021; Canfield et al., 2013; Ossa Ossa et al., 2018). Specifically, the FB_2 deposits aged 2092 ± 48 Ma (Ngwal'ghoubou Ikouanga, 2022) are composed of Poubara sandstones interbedded with thin black shale levels (FB_{2a} unit) and 5-m thick black shales with cm-thick siltstone layers (FB_{2b} unit) (Fig. 3). Lithofacies analyses indicated that the black shale deposits of FB_{2b} were emplaced in a calm, low-energy marine environment after a large discharge of sands (Reynaud et al., 2018). The relatively oxygenated water column, together with the cyanobacterial mats, may have favoured the development and preservation of complex macroorganisms (Aubineau et al., 2021, 2018; Canfield et al., 2013; El Albani et al., 2019a; Reynaud et al., 2018).

3. Materials and Methods

The studied specimens were collected from the FB_{2b} black shales. Four morphotypes of macrofossils, including different lobate-shaped, string-shaped, segmented, and lenticular-shaped forms, as well as microbial mat communities, described as mat-related structures (MRSs), are preserved throughout this entire rock unit (Aubineau et al., 2018; El Albani et al., 2019b, 2014, 2010). Ten specimens of each morphology (total of 40) were analysed.

The vertical distribution of the fossiliferous content is irregular (Fig. 3). While, the interbedded siltstones are completely devoid of macrofossils, MRSs have been described inside (Aubineau et al., 2018). Finally, pyrite concretions (Reynaud et al., 2018) were also found throughout the black shales. They are aligned in the lower part, are sparse and smaller in the middle part and form almost continuous pyritic beds in the upper part of the FB_{2b} unit. Polished slab sections were made for petrographic characterization at the macroscale. Microsamples were separated using a Dremel microdrill equipped with a diamond tip to precisely determine the mineralogical and chemical nature of the specimens. Specimens of all macrofossil morphological types were analysed: one unmineralized morphological type (round shape) and three mineralized types (lobed, tubular, and segmented shapes). For each of these

Code de champ modifié

types , the specimen (SP) and the host black shale (BS) have been characterized in detail. Pyritic concretions (clusters and nodules) present in the host black shales have also been investigated.

3.1. Petrographic observations

Petrographic observations of polished thin sections were performed to study the textural relationships, morphology, mineral assemblages, and chemical composition. Polished thin sections were first examined by a Nikon ECLIPSE E600 POL optical microscope coupled with a Nikon Digital Sight DS-U1 camera installed with NIS-Element D software. Selected polished thin sections were carbon-coated and examined using a JEOL JSM IT500 Scanning Electron Microscope at the University of Poitiers, France. The scanning electron microscopy (SEM) instrument was equipped with secondary electron (SE) and backscatter electron (BSE) detectors.

3.2. Bulk and clay mineralogy

The bulk and clay mineralogical compositions were obtained by X-ray diffraction (XRD) from randomly oriented bulk powders and oriented clay preparations, respectively, using conventional procedures (Brindley and Brown, 1980; Moore and Reynolds, 1997). The X-ray diffractograms were obtained using a Bruker D8 Advance diffractometer equipped with a copper source ($\lambda CuK\alpha = 1.5418$ Å). The analytical conditions were 40 kV and 40 mA; the acquisition parameters were 1 s with a step of 0.025 °2θ for angular ranges of 2-65 °2θ and 2-30 °2θ for randomly oriented powder and oriented clay samples, respectively. XRD patterns were deconvoluted in the 7-10° 2θ range using Fitik software to semiquantify mixed layer clay minerals (using peak areas).

4. Results

4.1. Macroscopic description of studied biotic and abiotic structures.

Here, we report a multiscale description of specimens previously described by El Albani et al. (2023, 2019b, 2014 and 2010).

4.1.1 Lenticular-shaped forms

The lenticular-shaped fossils look like subcircular capsules with a more or less pronounced central bulge (Fig. 4A-B). They can be found associated with other macrofossils (Fig. 4A), form aggregates overlapping each other, or are preserved alone (Fig. 4B). The diameters range from 0.3 to 5 cm. The inner surface comprises a core and a flat collar containing fine radial striations. The length of the collar represents 25% of the total radius. The observed shape of the lenticular fossils results from epirelief moulding, i.e., light silty and dark clayey laminae of the host sediments mould the specimens (convexity of laminae shown in Fig. 4C).

4.1.2. Lobate form

The lobate macrofossils are characterized by a rounded (Fig. 4D) or ovoid (Fig. 4E) inner part and an outer part composed of a succession of smaller lobes delimited by deep radial striae. The lengths of the specimens vary from 2 to 4 cm, and their widths vary from 1 to 2 cm. They are almost entirely mineralized by phenocrystal of euhedral pyrite (2 to 3 mm). The central lobes lack striae and may be more or less smooth. The lobes are mineralized, consisting of aggregates of euhedral pyrite grains (Fig. 4F). The mineralized specimens locally display a submillimetre-sized border of more "diffuse" pyrite, particularly at the lobed end - where smaller euhedral pyrite crystals are packed in a clay matrix - which rapidly fades at the outer edge of the specimen. At the contact zone between the specimens and host sediments, textural changes in the sediments are visible (Fig. 4F): the host sediment presents alternating light silty laminae and dark clay laminae that follow the border of the contact zone, suggesting that the host sediment was not consolidated at the time of fossil mineralization.

4.1.3. String-shaped forms

The string-shaped specimens have a millimetre-scale ovoid diameter and centimetre-scale elongated body fossils (Fig. 4G, H). The edges are clear (Fig. 4G) but may be bifid (Fig. 4H). They have been interpreted as multicellular organisms capable of moving vertically or horizontally with respect to the sediment to reach nutrients (El Albani et al., 2019a). The string-shaped structures are largely pyritized, but the remaining porosity is filled by a clayey material that is more abundant in the cores of the fossiliferous structures (Fig. 4I). The host black shale sediments are slightly deformed in the contact zone with the fossils.

4.1.4. Segmented forms

The segmented specimens, which are pyritized and often associated with pyritized MRSs, appear as segmented, sinuous cylinders (Fig. 5A). The length of such fossilized structures reaches several centimetres, while the maximum width is up to 2 cm. The segmented forms may have a homogeneous shape over the entire length, and a narrowing of a few millimetres has been observed. Pyritization is likely continuous between segmented fragments. Perpendicular to the elongation, cylindric fossils appear completely pyritized, although the core host septaria-type fractures are filled with a dark clayey matrix (Fig. 5B). Intergranular porosity is strongly reduced at the edges of segmented specimens.

4.1.5. Mat-related structures

Mat-related structures are ubiquitous in both black shale laminae and intercalated siltstone levels. Numerous mat morphotypes, up to 10, were formed by either mat growth or mat-protected patterns (Aubineau et al., 2018). The latter resulted from the mat preservation of abiotic structures. One of the

most common MRSs in the FB2b unit is the fairy-ring structure (Fig. 5C). In addition, the FB2b MRS may also be associated with macrofossils.

4.1.6. Pyritized mineral concretions

Mineral concretions consist of aggregates of euhedral pyrite phenocrystals that display specific morphologies. Concretions may form isolated clusters or discontinuous beds (Fig. 5D-E). The polished cross-section shows that the pyritization of concretions was intense where the crystal size increases from the core to the edge (Fig. 5F). Early small euhedral crystals likely served as templates for the later crystals, which are now observable. A reduction in the intergranular porosity is strongly apparent at the edges. While the light silty and dark clayey laminae of the host black shales are slightly deformed near the concretions, a general flexure following the overall structure is lacking. This suggests that the sediment was partially consolidated when the pyrite crystallized.

4.2. Mineralogy

4.2.1. Host sediments

Based on XRD data and SEM observations, the bulk mineralogy of the host sediments close to each fossil mainly consists of quartz and clay minerals (Fig. 6A-7A-8A). Carbonates, Do (peak at 2.89 Å – dolomite, and the peak is sometimes slightly shifted to 2.90 Å – dolomite-Fe-/ankerite), are minor, and pyrite, Py (peak at 2.71 Å), is in extremely low amounts. The clay fraction (Fig. 6B-7B-8B) is mainly composed of chlorite, C (characteristic peaks at 14.2 Å and 7.09 Å); illite/mica, I/M (at 10.00 Å); mixed layers of illite/smectite, MLs and MLi (~ 10.8 Å); and smectite, Sm (16.9 Å), to a lesser extent, which was identified after ethylene glycol saturation (Fig. 6C-7C-8C). This treatment also causes a slight shift towards higher 00l spacing and a reduction in the intensity of the ML peak coupled with an appearance of a shoulder at approximately 9.8 Å.

The deconvolution of the XRD patterns for mixed layer ML phases (Fig. 9A, Tab. 1-2) shows a clear contribution of an illite-rich term in mixed layers (MLi) at 10.3 Å, which may be slightly influenced by a term richer in illite (illite-like) at 10.1 Å. Assuming that the smectite interlayers are entirely occupied by divalent cations (Ca, Mg), one can approximate the I/S ratios in both types of ML: MLi (I=94%; S=6%) and MLs (I=80%; S=20%). In both cases, illite is always the dominant component of these mixed-layer minerals (Tab. 1).

4.2.2. Lenticular-shaped forms (nonpyritized macrofossils)

The lenticular-shaped forms are mainly filled by quartz (3.34 Å) associated with clay minerals (4.49 Å), dolomite (2.89 Å), and pyrite to a lesser extent (2.71 Å) (Fig. 6A). The clay fraction consists of chlorite (14.2 Å and 7.09 Å), illite/mica (10.0 Å), mixed layers of MLi and MLs, and discrete smectites (Fig.

264 6B-6C). The mixed-layer MLs are characterized by a d_{001} reflection centred at 10.9 Å after glycolation,
265 which corresponds to ordered MLs with the persistence of some smectite-rich layers (I=82%; S=18%).
266 Overall, the mineralogical assemblage is identical to the host sediment (Fig. 9B); the illite/smectite ratio
267 seems to be lower, indicating a lower illite content than in the sediment.

268 ***4.2.3. Pyritized fossils***

269 The lobate, string-shaped and segmented specimens are dominantly filled by pyrite (Fig. 7A). Quartz
270 and clay minerals are identified only after separation of the <2 µm clay fraction. The clay mineral
271 assemblage, consisting of chlorite, mixed layer MLi and MLs, and illite/mica, is similar to that of the
272 host black shale sediments (Fig. 7B). Nonetheless, smectite is present in the string-shaped structures
273 (Fig. 7C). The illite/(MLi) ratio is globally lower than that of the host sediment (Fig. 9B, Tab. 1).
274 Importantly, the main mineralogical differences between pyritized fossils and their host sediment are
275 the higher abundance of mixed layers compared to illite/mica combined with the absence of carbonates.

276 ***4.2.4. Pyritized concretions***

277 Unsurprisingly, these concretions are made of pyrite with few associated phases (Fig. 8A). Nonetheless,
278 chlorite, illite, mixed layers of MLi and quartz are observed in the ≤ 2 µm clay fraction (Fig. 8B-8C).
279 Unlike the sediment and all fossils, low amounts of MLi (10.3-10.4 Å), together with the lack of MLs,
280 characterize these concretions, as indicated by the high illite/MLi ratio (Fig. 9C, Tabs. 1-2).

281 ***4.3. Petrography***

282 ***4.3.1. Host sediments***

283 Along the stratigraphic sequence of the Moulendé quarry, the host sediments always consist of a clay
284 matrix, quartz, chlorite, pyrite, and dolomite, as illustrated by XRD data and SEM observations (Fig.
285 10). The clay phase proportion varies according to the granulometry of the laminae. The clayey facies
286 (Fig. 10A) correspond to deposits of a densely packed clayey matrix with chlorites, disseminated pyrite
287 and rounded to subangular quartz grains densely packed. The transitional facies – composed of silty clay
288 (Fig. 10B) or clayey silt (Fig. 10C and 10D) – is marked by an increase in the grain size of quartz and
289 chlorite. Compared to the clayey facies, the quartz morphology here is closer to polycrystalline
290 aggregates. Chlorites display three 2-D morphologies, including lamellar structures, rectangular
291 platelets, and ovoidal shapes, which can exceed 50 µm in length and diameter (Fig. 10A-10B-10). In all
292 cases, the particles are composed of poly-lamellar stacks. In addition, the edges of the ovoids show thick
293 grey halos, probably due to iron depletion from postdepositional alteration and/or recrystallization
294 processes. The porosity can be filled by intertwined or stacked secondary chlorite lamellae, which
295 developed at grain contacts with primary phases (quartz, chlorite in platelets) or as coatings (Fig. 10D).
296 In these facies, pyrite is either disseminated, corresponding to euhedral to subeuhedral crystals, or

intergrown with chlorites (Fig. 10C). Although pyrite is a minor phase, its proportion is higher than in the clayey facies.

4.3.2. Nonpyritized macrofossils: Lenticular-shaped forms

The clay material of the lenticular-shaped forms is mainly filled by illite particles, while quartz grains are scarce (Fig. 10E). On the other hand, chlorites in flexuous lamellae, oriented parallel to the stratification, seem to be much more abundant than in the sediments, although chlorite with platelet and ovoid shapes are present in low amounts. The size (10 to 20 µm) of the latter is generally smaller than that of the host sediment. Finally, tiny anhedral, disseminated pyrite grains are observed.

4.3.3. Pyritized fossils

Clayey assemblages identified by XRD fill the intergranular pores between pyrite crystals that preserved the mineralized macrofossils, while detrital minerals (e.g., quartz, primary chlorite, and dolomite) are almost absent (Fig. 10F-10G).

The lobate, string-shaped, and segmented specimens are essentially composed of illite I/M (Fig. 10F). Micrometric illite (I/M) is mainly in the form of stacked sheets (Fig. 10) and shows signs of free growth within the pore spaces. Chlorite has developed as short platelets in the intragranular porosity, probably at the expense of illite as encompassing relict patches of illitic matrix (Fig. 10F). Inside the porosity, chlorite lamellae are interbedded with illite as “accordion” structures. Secondary quartz patches are also observed (Fig. 10G).

4.3.3. Pyritized mineral concretions

Pyrite concretions has allowed the development of strongly interlocking pyrite phenocrystals, reducing the porosity (Fig. 10H-10I). The clay assemblage that fills the residual porosity of plated concretions seems to be diagenetic considering their size and shape, and does not contain an illite-rich matrix. In the nodules, part of the porosity is occupied by the illite. However, chlorite is more abundant than illite (Fig. 10I).

5. Discussion

Processes impacting soft-bodied organism preservation

Studying the degree of conservation of biological bodies is essential for understanding taphonomy. Moreover, it is of great interest to elucidate the environmental conditions and taphonomic mechanisms that prevailed during the different stages of preservation (Behrensmeyer et al., 2000).

The preservation of soft bodies involves sufficiently slow biological degradation for the more resistant organic molecules to be fossilized by imprinting or mineralization (Briggs, 2003). The early stage of

preservation is mainly controlled by the nature of the sediments and their rate of accumulation (Briggs and Kear, 1993) in the presence or absence of biological agents (bacteria) together with the water column chemistry (major elements, dissolved O_2, etc.) of the depositional environment (Gaines et al., 2012; Gaines and Droser, 2010). Compaction, cementation, fluid–rock interaction, and potential hypothermal and magmatic activities can also impact the quality of fossilization (Muscente et al., 2015).. Such parameters have a direct impact on reconstructing the initial form of soft-bodied organisms and deriving information on their lifestyles based on the geometric (morphologies, tracks, burrows, etc.) and chemical (organic molecules, isotopes, etc.) signatures that have been preserved.

Taphonomic information from pyritization

As previously presented, in the FB_{2b} formation (El Albani et al., 2010, 2014, 2019, Aubineau et al. 2019), pyritization is not specific to the body fossils but is also associated with abiotic concretions in the host black shales throughout the stratigraphic sequence. This is expected because the black shale sediments contained sufficient organic matter and iron to promote pyritization independently of the carbon origin (Canfield et al., 2013). Petrographic observations of lenticular nonpyritized specimens indicate that moulding materials are inherited from the host sediments. The similarity of the detrital and diagenetic clay materials in both the host sediments and lenticular infilling is not observed when pyritized macrofossils and their associated host sediments are compared.

Pyritization of soft bodies related to bacterial sulfate reduction (Gabbott et al., 2004) can occur when organic biodegradation is relatively rapid (Briggs et al., 1996) and takes place in clay-rich sediments (Farrell, 2014) under the oxic–anoxic interface (Berner, 1984). Under these conditions, the formation of hydrogen sulfide and the occurrence of reactive iron concentration gradients in or around the labile organic matter of dead organisms (Guan et al., 2017) favour the nucleation of iron sulfide (Allen, 2002) or iron-rich clays (Petrovich, 2001). Rapid organic matter remineralization produces carbon dioxide (or methane) and water. The degradation rate is a function of several factors, such as (i) the physico-chemical properties of the sediments, (ii) the characteristics of the decomposing organic matter, and (iii) the microbial populations involved (Muscente et al., 2017). In the studied case, the coexistence of different taphonomic styles in the same sedimentary laminae cannot be explained by variations in criteria (i) and/or (ii). On the other hand, the speed of degradation can play an important role in favouring biomineralization. This mechanism depends on the biodegradability of the main molecular compounds (carbohydrates, lipids, proteins) of the organic matter (*e.g.*, (Stankiewicz et al., 2000), i.e., their ability to be photodegraded, hydrolysed or incorporated into the biomass by serving as nutrients for microorganisms (Briggs, 1999). Rapidly decomposing organic matter, known as labile material, is easily attacked by enzymatic catabolism, and its chemical constituents are easily reused by microbial metabolism. In contrast, the organic materials that are part of the composition of structural bodies

(envelopes, partitions, etc.) can be recalcitrant to decomposition (*e.g.*, Butterfield, 2003; Tegelaar et al., 1989).

Taphonomic information from clay minerals and their evolution during diagenesis

The Francevillian biota lived in a shallow marine environment where periodically resuspended fine particles eventually sedimented into fine-grained laminae (Reynaud et al., 2018) in an oxic to suboxic water column (Aubineau et al., 2021; Canfield et al., 2013). The finely laminated horizons are composed of quartz and clay minerals associated with low amounts of dolomite and pyrite. The primary clay mineralogical assemblage of Francevillian sediments evolved differently depending on whether it was located within the preserved specimens by (i) simple compression casting or by (ii) mineralization (biogenic or abiotic). The former mechanism can be compared to the Burgess Shale-type preservation (Butterfield, 1995; Gaines et al., 2005) but without the overprint of metamorphism. Regardless of the preservation mechanism, all macrofossils are in laminae where clayey microfacies prevail in overall low-permeability rocks. This suggests a direct relationship between the nature of the original organism, its taphonomy, and the rock morphological elements that have been preserved.

The degree, condition, and mechanism of fossil preservation are strongly controlled by mineral transformations and/or neo-formations, particularly clay minerals (e.g., (Anderson et al., 2011; Gabbott et al., 2001; Martin et al., 2004) and associated phases (sulfides, carbonates, etc.). During early diagenesis, anoxic microenvironments develop in association with organic matter degradation; Fe^{2} ions adsorbed on the preserved biopolymers may favour nucleation of crystals of iron(II)-rich clay minerals (berthierine or ferroan saponite), which form a coating on the organic remains and/or replace parts of the organism (Petrovich, 2001). Nevertheless, these minerals associated with both pyritized and nonpyritized specimens evolve during burial diagenesis, leading to the formation of new phases inherited from their initial chemical composition. Therefore, the specific study of these minerals is justified to reveal the conditions and mechanisms of fossil preservation in ancient sediments.

At the millimetre to centimetre scale of the fossil microsites and their host sediments, the dominant mechanism of clay mineral transformation associated with the early stages of preservation of Francevillian soft-bodied organisms is illitization. This authigenesis is represented first by smectite *sensu stricto* and then smectite-rich mixed-layer illite/smectite, namely, MLs. Since only a few MLs are still preserved, extensive illitization occurred. The intensity of this mechanism is primarily controlled by the potassium availability in the system (Cuadros and Linares, 1996). Considering the absence of K-feldspars and evidence of K-rich fluids in the study area, the K supply is of paramount importance. Near the surface, dissolved potassium in the overlying water column was theoretically available (Santiago Ramos et al., 2018; Sun et al., 2015). However, seawater's sodium concentration and ionic strength are not very favourable for direct solid-solution exchange and absorption of potassium in the interlayer spaces of swelling minerals (smectites and illite/smectite mixed layers). Alternatively, potassium may

399 have been supplied by the degradation of MRSs that naturally fixed K for cellular machinery (Aubineau
400 et al., 2019). The latter mechanism, in the marine environment, has long been known to regulate
401 microorganism growth and cellular osmotic pressure (Rhoads and Epstein, 2003) and to collaborate in
402 many metabolic reactions, such as protein synthesis and enzyme activation (Stautz et al., 2021). Thus,
403 a similar mechanism of K concentration can be argued for bacteria that degrade the organic matter of
404 dead organisms, which is the most plausible explanation. In this case, heterotrophic microbial respiration
405 degrading the organic matter would have promoted K release and concentration in the interstitial pore
406 waters of the unconsolidated sediments. This K increase would have favoured the conversion of swelling
407 smectite into MLs in the early stages of burial and, ultimately, illite, which would correspond to induced
408 biogenic mineralization. Despite the presence of K in the marine system, in both cases, the end of
409 bacterial activity stopped K accumulation in the preserving microsystem and thus reduced the illitization
410 mechanism.

411 Illitization is a general mineral transformation that affects both the host sediments and the studied
412 specimens. This mechanism involves the transformation of MLs into MLi as transitional phases and
413 then into illite. Nevertheless, the degree of this transformation is variable regarding the proportion of
414 illite–MLi–MLs phases. When the K content was sufficient, the MLi could be completely transformed
415 into illite-like and/or illite phases. However, here, all samples have remaining MLs and/or MLi. In the
416 case of the nonpyritized fossils, illitization was not achieved, as testified by the preservation of
417 illite/smectite mixed layers (MLs) and the lower illite/MLi ratio. The same occurred in the pyritized
418 specimens, but illitization was more intense, i.e., a higher illite/MLi ratio, except for segmented forms.
419 For other forms, the host sediments present higher illite/MLi ratios than fossils, while the pyrite
420 concretions show MLi that is very enriched in K and a higher illite/MLi ratio. These heterogeneous
421 results highlight that each fossil represents a microsystem whose location, nature and rate of degradation
422 influence the availability of potassium, controlling the intensity of illitization.

423 The illitization mechanism was followed by chloritization, as shown by the development of secondary
424 chlorites from the microcrystalline illitic matrices and/or recrystallized MLi in “accordion-like"
425 structures. The presence of many chlorite shapes is due to the mixing of primary and secondary phases
426 (Fig. 10). In the fossils, ovoids and laths are observed in low amounts on the outer rims associated with
427 reduced porosity and are absent in the central part. Conversely, “accordion-like” structures and radial
428 shapes are much more abundant in the central parts of the pyritized specimens but absent in the
429 nonpyritized circular forms.

430 In host sediments and fossils, chlorite shapes indicate different origins. Ovoid forms are clearly detrital.
431 The other shapes are probably secondary products from direct precipitation (fibroradial) or from
432 transformation of a precursor (accordion-like shapes). In the latter case and in the illitic clay matrix,
433 chloritization seems to be developed at the expense of the smectitic part of the clay phases and
434 encapsulates residual S–MLs–MLi. Under these conditions, both transformation and

435 dissolution/precipitation mechanisms are probably involved. In contrast, in the concretions,
436 chloritization results from direct precipitation in a free pore space, leading to the development of
437 chlorite-dolomite paragenesis in the intergranular porosity. Regardless of the study area, chloritization
438 occurred after the early phase of illitization and during burial diagenesis, benefiting from fluid
439 circulation that supplied the necessary Fe and Mg.

440

441 ***Towards a taphonomic conceptual model***

442 Our results allow us to summarize the taphonomic history by a conceptual model (Fig. 11), describing
443 the fossilization stages of each type of specimen within a microsystem.

444 After their death, the specimens are deposited on clayey sediment that is mainly composed of quartz,
445 clay minerals, small amounts of dolomites and pyrite. The specimens are quickly buried within specific
446 microenvironments, where all of the fossilization mechanisms take place. In this way, lenticular
447 specimens undergo nonpyritized fossilization, while the lobed, segmented and tubular forms are
448 pyritized.

449 After decomposition of the organism's body, lenticular forms are trapped in a sediment that is still loose
450 but coherent enough to maintain the mould. The voids left by decomposition are progressively filled by
451 particles via size sorting, favouring a high concentration of fine material within the specimen.

452 The mode of fossilization of the pyritized forms is approximately identical. After their deposition, the
453 specimens are degraded progressively by sulfate-reducing bacteria during burial activity. The
454 conservation of the specimens is conditioned by the speed of degradation of the internal structures and
455 favoured by the bacterial activity. Early pyritization permits 3D preservation of each specimen.

456 After this early stage of fossilization, a secondary diagenetic overprint participates in the stabilization
457 of the specimens. This is represented by the illitization of the smectitic phases. This illitization is
458 controlled by the availability of K and the permeability of each microsystem. Due to the high
459 concentration of finer materials, nonpyrite specimens present microsystems in which exchanges with
460 the outside are more reduced compared to pyrite specimens and concretions. The intensity of the
461 illitization reaction increases progressively from the nonpyritic forms to the abiotic concretions through
462 the pyritic specimens. These microsystems are later subjected to generalized chloritization, reflecting
463 the circulation of fluids rich in Fe and Mg. Abiotic pyrite concretions are formed during late diagenesis.

464 As summarized here, our data provide robust evidence that clay minerals, such as smectite, illite,
465 illite/smectite mixed layers, and chlorite, can be used as indicators for the physico-chemical changes
466 that occur at the local scale during the preservation of soft-bodied organisms.

6. Conclusion

The 2.1 Ga Francevillian fossils preserved in black shales show two early preservation modes corresponding to moulding/compression and pyritization. In the pore spaces of the sediments and fossils, the mechanisms of clay transformation associated with the evolution of the system are successively illitization and chloritization. The intensity of these processes and the habit of the authigenic clay minerals depend on the degree of porosity and key element availability, such as K. Thus, the intensity of illitization at the early stage differs between the sediment, pyritized and nonpyritized fossils and pyrite concretions of the same age. The potassium availability may have been controlled by the microbial activity of bacterial mats everywhere in the black shale levels, leading to the biodegradation of organic matter from soft bodies. In this scheme, each fossil represents a microsystem. At a late stage, chloritization begins, and its intensity is determined by the contents of soluble iron and magnesium from fluid circulation.

In the same depositional setting, we observe heterogeneous clay mineralogical assemblages, depending on the presence or absence of organic matter remains. We also observe contrasting clay mineralogy by comparing biotic and abiotic pyritized specimens. In fact, preservation (moulding and pyritization) occurred within microsites, whose properties significantly impacted the clay mineral reactions, which cemented the pore spaces and thus contributed to the final fossilization. Fossil microsites must be considered microsystems that have undergone physical and chemical changes that are different from those of their immediate surrounding environment, which is similar to additional indirect evidence of the existence of biological remains encapsulated in the sediment. These data could represent a diagnostic tool for detecting traces of life in rocks from the early Earth.

Author Contributions: A.E.A. designed the research. A.E.A., J.N.I., C.F and F.B. wrote the manuscript. A.E.A, J.N.I, O.B., A.T and C.L. did the field work. J.N.I., C.F., A.M., A.A.E., A.R. and A.E.A. prepared the samples and performed XRD analyses and models. L.R., A.C.W. Performed Re/Os datations.

Acknowledgment

Funding was provided by La Region Nouvelle Aquitaine, French Embassy at Libreville (Gabon). They are acknowledged for their support and collaboration. The authors are also grateful to the National Agency of National Parcs, le CENAREST, Socoba BTP for their assistance and access to the localities. We appreciate C. Lebailly, R. Oslisly, J.L. Albert, C. Boissard, L.Tromas S. Ventalon, J.C. Baloche for their assistance and support.

Table 1 – Ratios of areas of d_{001} reflections of illite/mica and illite/smectite mixed-layers rich in illite, measured from diffractogram patterns of air-dried oriented preparations.

Host sediment and specimen associated		Major peak area		
		Illite (10.0 Å) (cts.°2q)	MLi (≈10.5 Å) (cts.°2q)	Ratio Aillite/AMLi
Circular (R)	max.	469	3774	0.12
	min.	215	3654	0.06
Lobated (L)	max.	658	2719	0.24
	min.	118	1100	0.11
Segmented (S)	max.	1540	3664	0.42
	min.	41	2303	0.02
Tubular (T)	max.	1475	1432	1.03
	min.	578	2706	0.21
Concretions (Co)	max.	119	42	2.85
	min.	427	1603	0.27

Table 2 – Semi-quantitative overview of the mineralogy of the clay phases based on XRD analysis and deconvolution of diffractograms. Empty circles: traces.

		Smectite *s.s.*	**MLs**	**MLi and Illite like**	**Illite *s.s.* Mica**
Host rock		○	○	●●	●●●
Lenticular fossil	*non pyritized*	●●	●●●	●●●●	○
Lobate fossil	*pyritized*	●	●●	●●●	●
Segmented fossil	*pyritized*	●	●●	●●●●	○

Tubular fossil	*pyritized*	●	●●	●●	●
Concretions	*pyrite*		●	●	●●

Figure 1 – Geological map of the Franvcevillian Basin (Gabon).

Figure 2 – Geological section showing the structure and the lithostratigraphic sequence of the Francevillian deposits on the northern edge of Mvengué syncline.

Figure 3 – Lithostratigraphy of the studied section (Moulendé quarry).

Figure 4 – Photographs showing the spatial relations between: **A)** pyritized lobate (pl) and non-pyritized lenticular shaped specimens. Arrows represent at top left a lenticular-shaped specimen and pyritised specimen at the right side. **B)** top view and **C)** cross section of unpyritized lenticular-shaped specimen. Arrows represent a sharp limit between a lenticular-shaped specimen and host-sediment. **D)** pyritized round lobated shapes, **E)** pyritized oval lobated shape, **F)** cross-section of a pyritized lobated shape. Arrows represent a sharp limit between the pyritized specimen and host-sediment with the evidence of pre-compaction. **G)** simple tubular shape, **H)** bifid tubular shape, **I)** cross-section of tubular shape. Abbreviations: (SP) specimen, (BS) black shale. Scale 1 cm.

Figure 5 – Photographs showing: **A)** pyritized segmented shape in contact with the bacterial mat (arrow), **B)** cross-section of segmented shape. Arrow represent the sharp and pre-compactional limit between specimen and host-sediment. **C)** Fairy ring structure type of bacterial mat (Aubineau et al 2018), **D)** plated coarse pyrite concretion, **E)** top view and **F)** cross-section of nodular pyrite concretion. Arrow represent the contact between coarse pyrite crystals cross-cutting the host-sediment. Abbreviations: (SP) specimen, (BS) black shale host. Scale 1 cm.

Figure 6 – **A)** Powder diffractograms showing bulk mineral composition of the host sediments and non pyritized macro-fossils (ciculars), **B)** Diffractograms of oriented air-dry preparations **C)** Diffractograms of oriented preparations after ethylene glycol solvation. Minerals: (C) Chlorite, (Do) Dolomite, (I/M) illite and/or Mica, (MLi) Mixed-layer illite-rich, (MLs) Mixed-layers smectite-rich, (Py) Pyrite, (Q) Quartz.

Figure 7 – **A)** Powder diffractograms showing the bulk mineral composition of the host sediments and pyritized macro-fossils (lobates, tubulars and segmenteds), **B)** Diffractograms of oriented air-dry preparations **C)** Diffractograms of oriented preparations after ethylene glycol solvation. Minerals: (C) Chlorite, (Do) Dolomite, (I/M) illite and/or Mica, (MLi) Mixed-layer illite-rich, (MLs) Mixed-layers smectite-rich, (Py) Pyrite, (Q) Quartz, (Sm) Smectite.

Figure 8– **A)** Powder diffractograms showing the bulk mineral composition of the host sediments and concretion, **B)** Diffractograms of oriented air-dry preparations and **C)** Diffractograms of oriented preparations after ethylene glycol solvation. Minerals: (C) Chlorite, (Do) Dolomite, (I/M) illite and/or Mica, (MLi) Mixed-layer illite-rich, (MLs) Mixed-layers smectite-rich, (Py) Pyrite, (Q) Quartz, (Sm) Smectite.

Figure 9 – Examples of diffractograms deconvolution obtained with air-dried oriented preparation of: (**A**) host sediment, (**B)** macrofossil samples, and **(C)** concretion. Distribution of clay minerals

554 proportions in quaternary plot with illite (I), Chlorite (C), Mixed-layers smectite-richer (MLs) and
555 illite-rich (Mli) end-members. Minerals: (C) Chlorite, (I) Illite and (MLi) Mixed-layers illite-rich
556 and/or illite-like, (MLs) Mixed-layers smectite-rich.

557 **Figure 10 –** Micrographs in backscattered electron (BSE) of the host sediments **(A, B, C, D)**, non-
558 pyritized macrofossils **(E)**, infilling of intergranular porosity of pyritized macrofossils **(F, G)**, and
559 infillings of intergranular porosity of plated **(H)** and nodular **(I)** pyrite concretions. Abbreviations: (C)
560 Chlorite, (Do) Dolomite, (IM) Illite/Mica, (MA) Undifferentiated Clay Matrix, (Py) pyrite, (Q) Quartz.

561 **Figure 11 –** Conceptual model illustrating the taphonomy and mechanisms of mineralization during
562 burial diagenesis.

563

564

Figure 1:

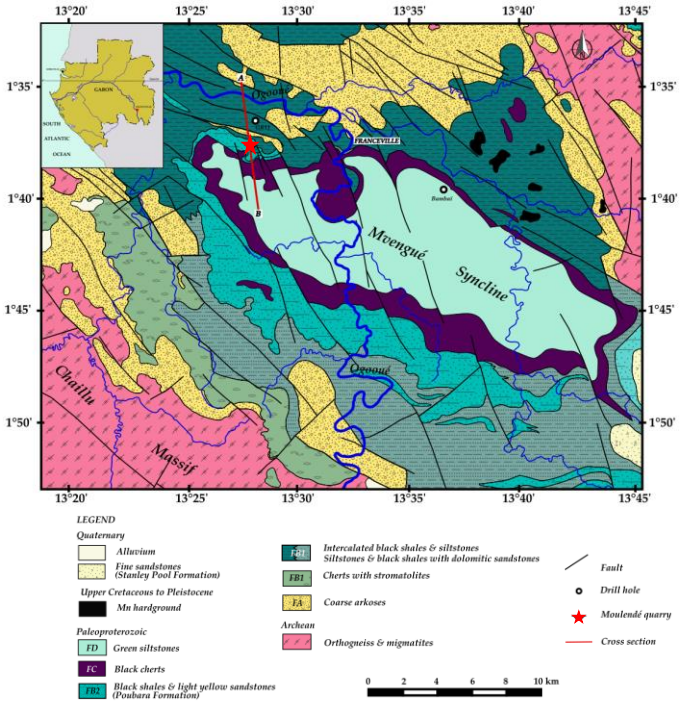
13°20'
13°25'
13°30'
13°35'
13°40'
13°45'
1°35'
1°40'
1°45'
1°50'
Mvengué
Syncline
Chaillu
Massif
Ogooué
FRANCEVILLE
Bamboni
LEGEND
Quaternary
Alluvium
Fine sandstones (Stanley Pool Formation)
Upper Cretaceous to Pleistocene
Mn hardground
Paleoproterozoic
FD Green siltstones
FC Black cherts
FB2 Black shales & light yellow sandstones (Poubara Formation)
FB1 Intercalated black shales & siltstones
Siltstones & black shales with dolomitic sandstones
FB1 Cherts with stromatolites
FA Coarse arkoses
Archean
Orthogneiss & migmatites
Fault
Drill hole
Moulendé quarry
Cross section
0 2 4 6 8 10 km

582 **Figure 2**

583

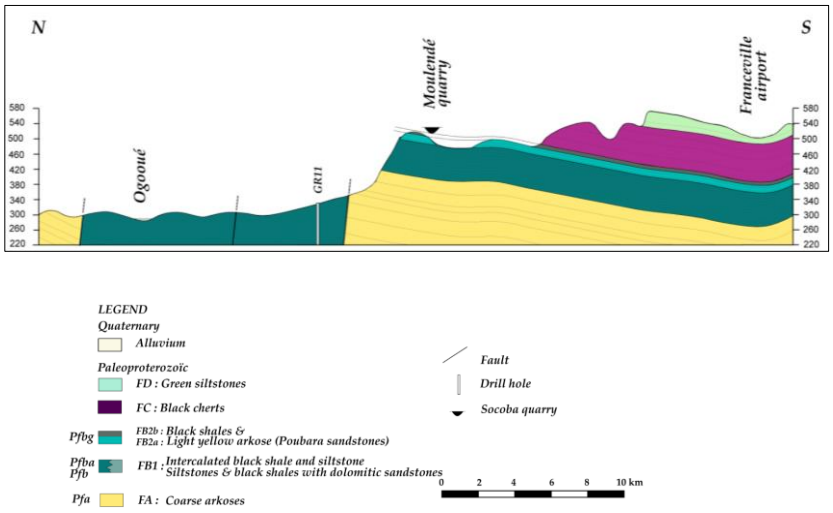

Figure 3

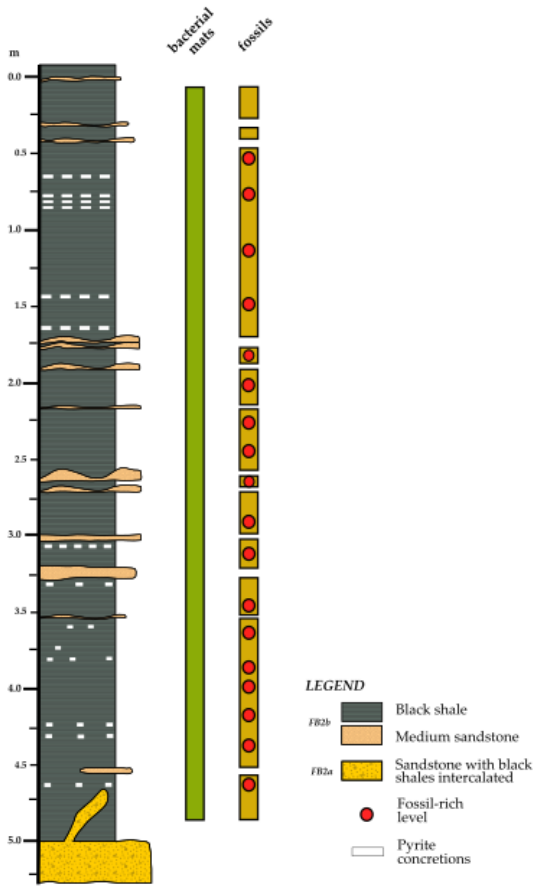
bacterial mats
fossils
m
0.0
0.5
1.0
1.5
2.0
2.5
3.0
3.5
4.0
4.5
5.0
LEGEND
FB2b
Black shale
Medium sandstone
FB2a
Sandstone with black shales intercalated
Fossil-rich level
Pyrite concretions

Figure 4

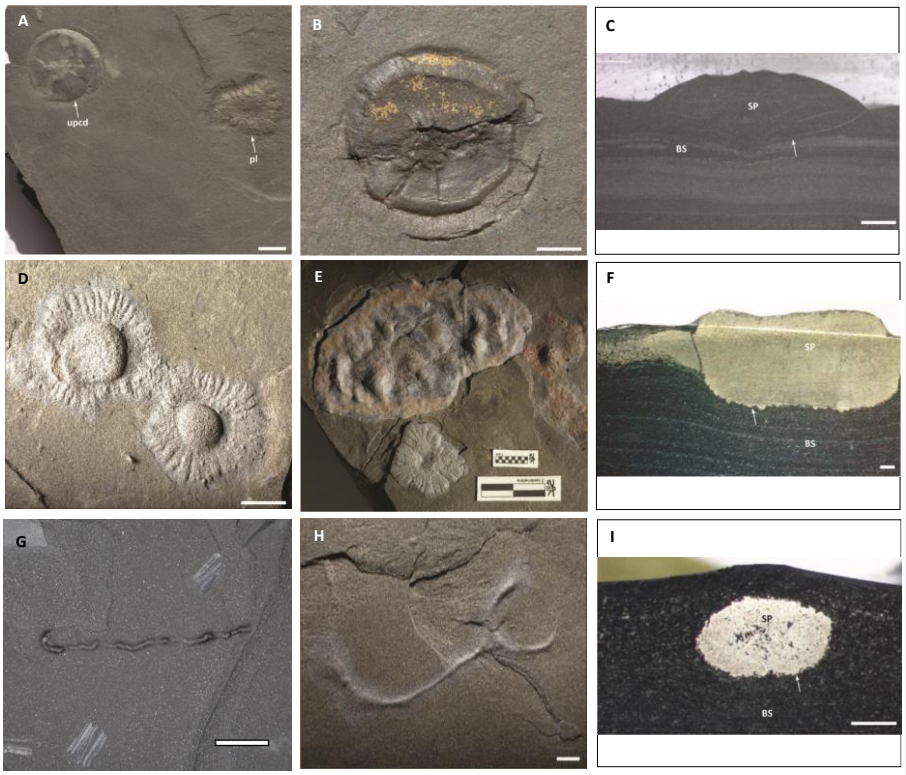

626 **Figure 5**

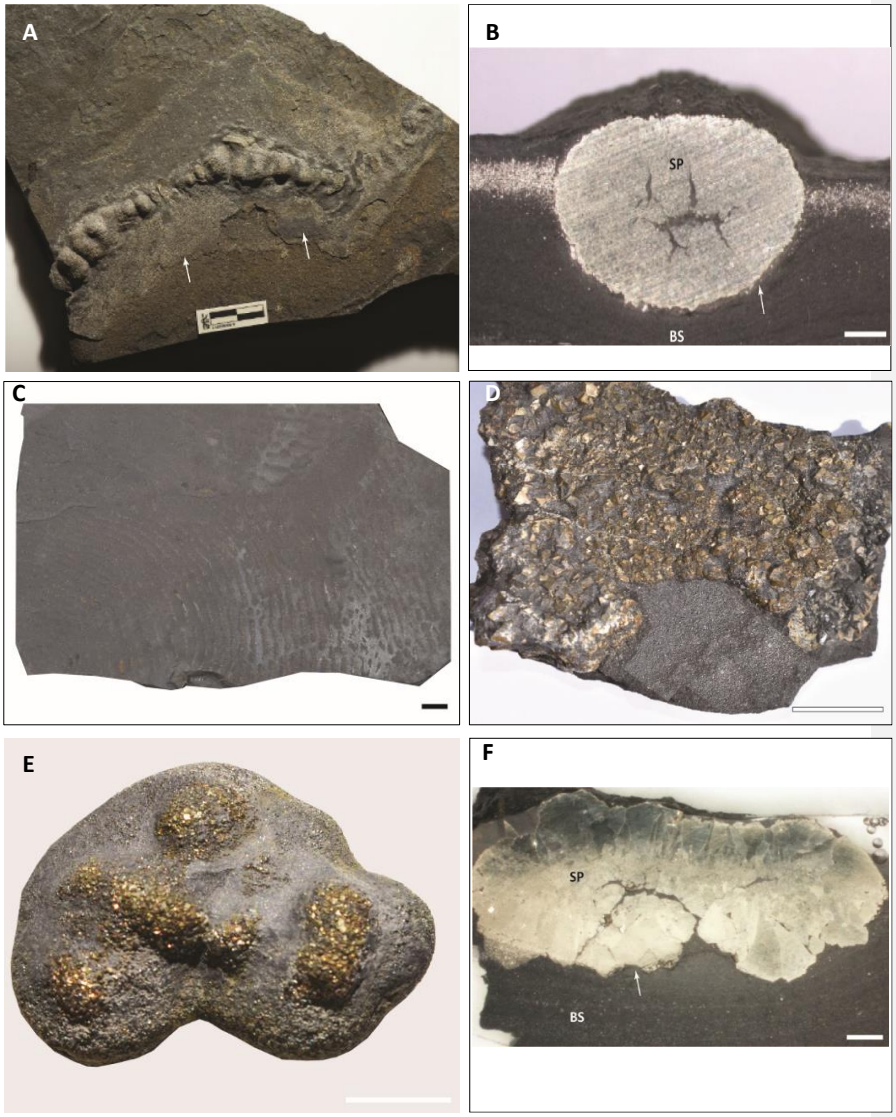

627

628

629

630

631

Figure 6:

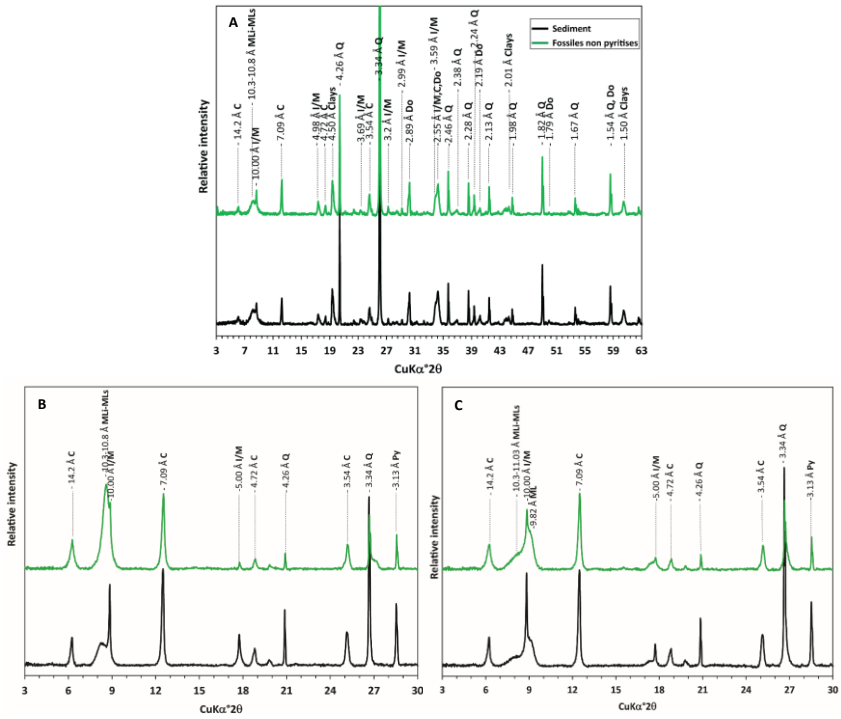
A
Sediment
Fossiles non pyritises
Relative intensity
14.2 Å C
10.3-10.8 Å Mi-Mls
10.00 Å I/M
7.09 Å C
4.98 Å I/M
4.72 Å C
4.50 Å Clays
4.26 Å Q
3.69 Å I/M
3.54 Å C
3.34 Å Q
3.2 Å I/M
2.99 Å I/M
2.89 Å Do
2.55 Å I/M,C,Do
3.59 Å I/M
2.46 Å Q
2.38 Å Q
2.28 Å Q
2.19 Å Do
2.24 Å Q
2.13 Å Q
1.98 Å Q
2.01 Å Clays
1.82 Å Q
1.79 Å Do
1.67 Å Q
1.54 Å Q, Do
1.50 Å Clays
CuKα*2θ
B
Relative intensity
14.2 Å C
10.00 Å I/M
10.8 Å Mi-Mls
7.09 Å C
5.00 Å I/M
4.72 Å C
4.26 Å Q
3.54 Å C
3.34 Å Q
3.13 Å Py
CuKα*2θ
C
Relative intensity
14.2 Å C
10.3-11.03 Å Mi-Mls
10.00 Å I/M
9.82 Å Mi
7.09 Å C
5.00 Å I/M
4.72 Å C
4.26 Å Q
3.54 Å C
3.34 Å Q
3.13 Å Py
CuKα*2θ

Figure 7:

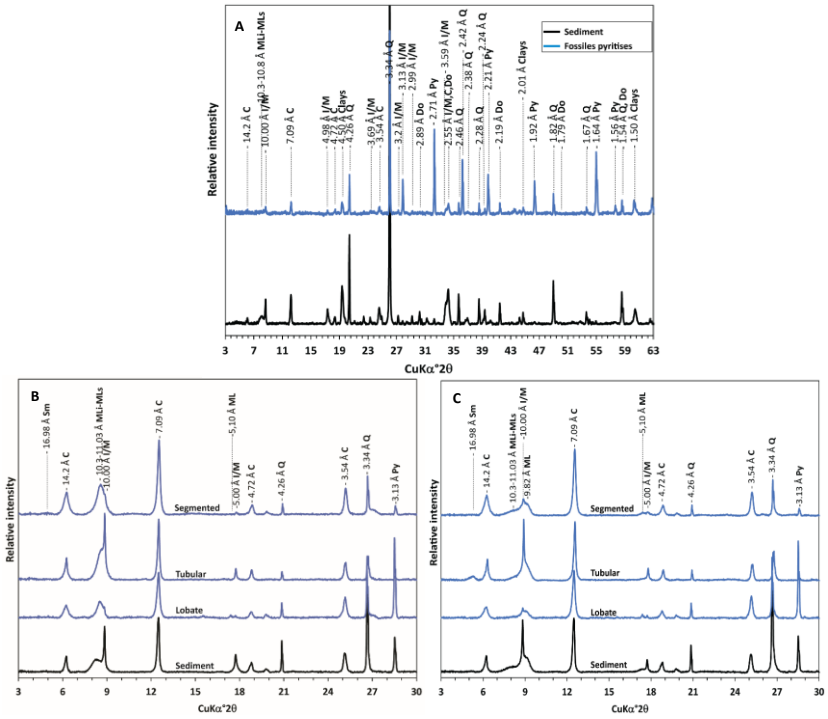
A
Sediment
Fossiles pyritises
Relative intensity
14.2 Å C
10.00 Å I/M
10.3-10.8 Å MLI-MLs
7.09 Å C
4.98 Å I/M
4.72 Å C
4.58 Å Clays
4.26 Å Q
3.69 Å I/M
3.54 Å C
3.34 Å Q
3.2 Å I/M
3.13 Å I/M
2.99 Å I/M
2.89 Å Do
2.71 Å Py
2.55 Å I/M,Cbo
2.46 Å Q
3.59 Å I/M
2.42 Å Q
2.38 Å Q
2.28 Å Q
2.24 Å Q
2.21 Å Py
2.19 Å Do
2.01 Å Clays
1.92 Å Py
1.82 Å Q
1.79 Å Do
1.67 Å Q
1.64 Å Py
1.56 Å Py
1.54 Å Q, Do
1.50 Å Clays
3 7 11 15 19 23 27 31 35 39 43 47 51 55 59 63
CuKα°2θ
B
16.98 Å Sm
14.2 Å C
10.3-11.03 Å MLI-MLs
10.00 Å I/M
7.09 Å C
5.10 Å ML
5.00 Å I/M
4.72 Å C
4.26 Å Q
3.54 Å C
3.34 Å Q
3.13 Å Py
Segmented
Tubular
Lobate
Sediment
Relative intensity
3 6 9 12 15 18 21 24 27 30
CuKα°2θ
C
16.98 Å Sm
14.2 Å C
10.3-11.03 Å MLI-MLs
10.00 Å I/M
9.82 Å ML
7.09 Å C
5.10 Å ML
5.00 Å I/M
4.72 Å C
4.26 Å Q
3.54 Å C
3.34 Å Q
3.13 Å Py
Segmented
Tubular
Lobate
Sediment
Relative intensity
3 6 9 12 15 18 21 24 27 30
CuKα°2θ

Figure 8:

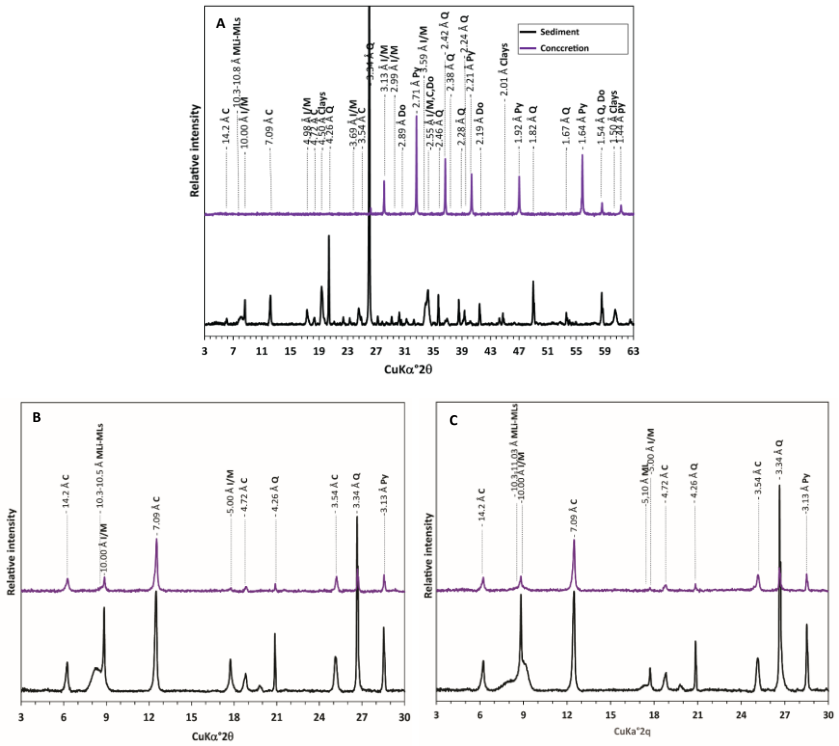
A
Sediment
Conccretion
Relative intensity
CuKα°2θ
B
Relative intensity
CuKα°2θ
C
Relative intensity
CuKa°2q

664 **Figure 9:**

665

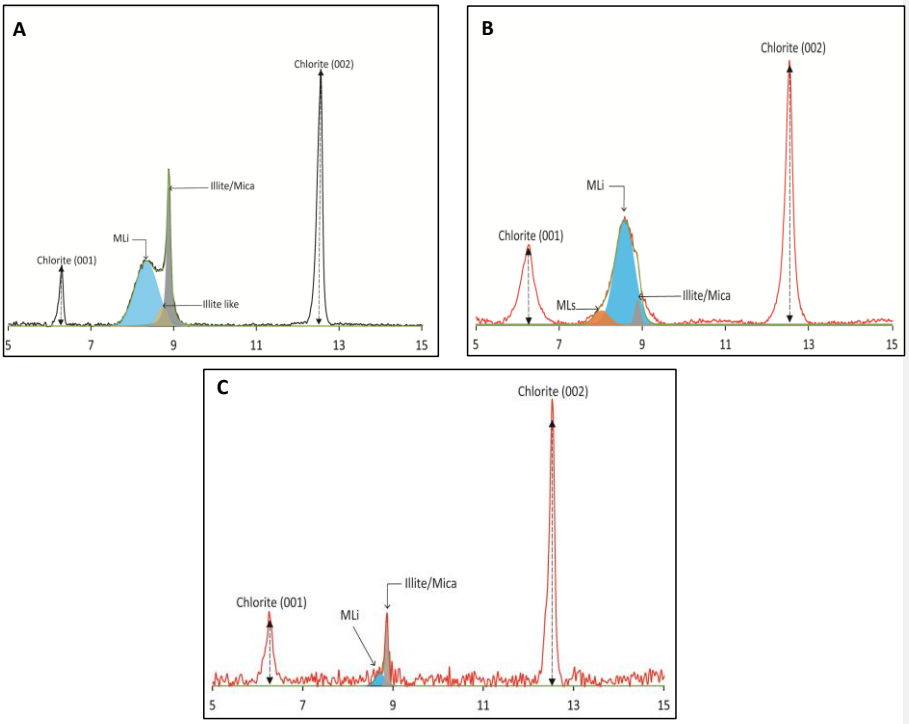

666

667

668

669 **Figure 10:**

670

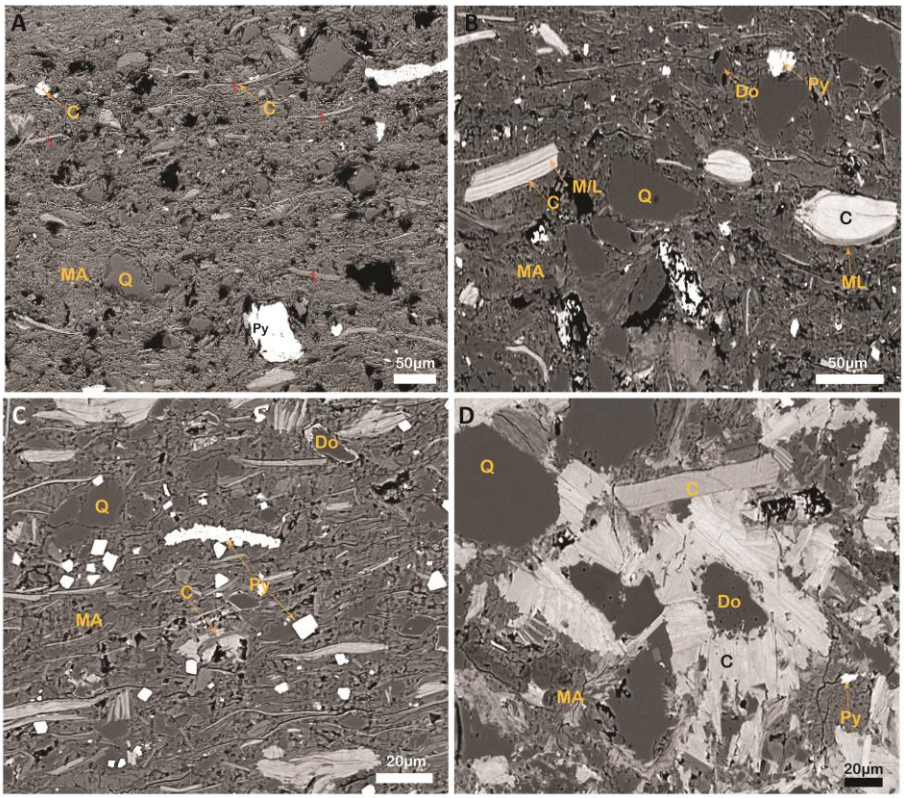

671

672 **Figure 11 (Suite)**

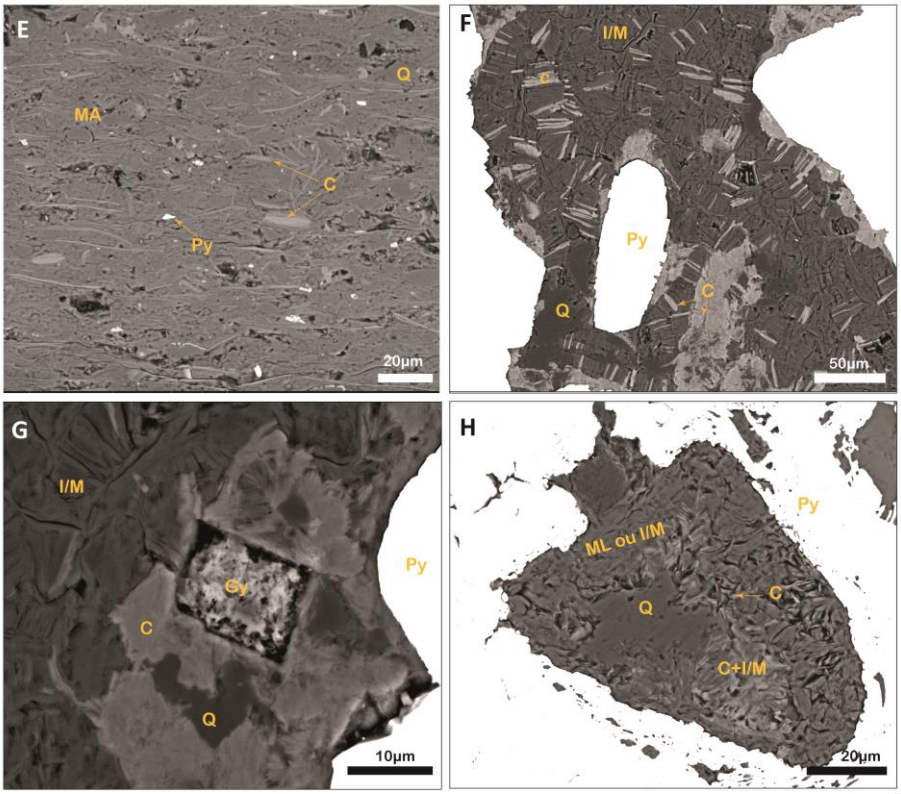

673

674

Figure 11 (suite)

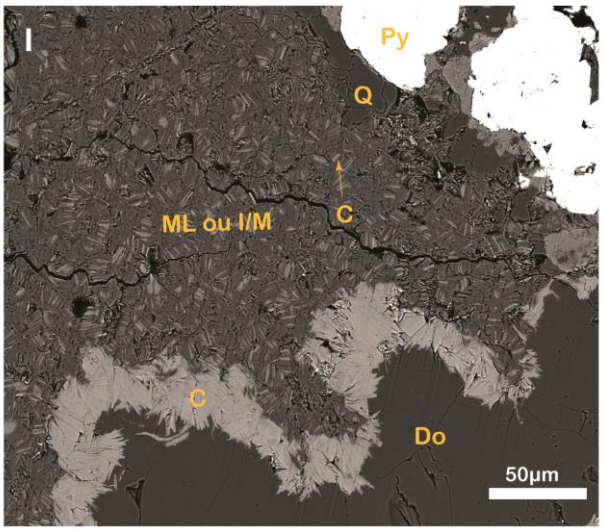

698 **Figure 12**

699

700

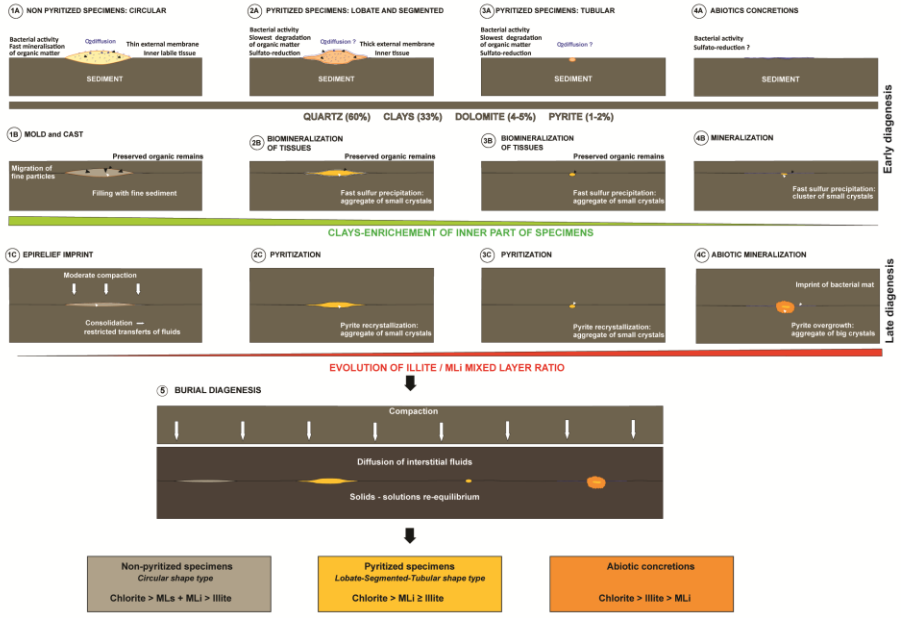

701

References

Allen, R.E., 2002. Role of diffusion–precipitation reactions in authigenic pyritization. Chemical Geology 182, 461–472. https://doi.org/10.1016/S0009-2541(01)00334-5

Anderson, E.P., Schiffbauer, J.D., Xiao, S., 2011. Taphonomic study of Ediacaran organic-walled fossils confirms the importance of clay minerals and pyrite in Burgess Shale−type preservation. Geology 39, 643–646. https://doi.org/10.1130/G31969.1

Aubineau, J., Bankole, O.M., Baron, F., Grégoire, B., El Albani, A., 2021. Authigenic kaolinite and sudoite in sandstones from the Paleoproterozoic Franceville sub-basin (Gabon). Comptes Rendus. Géoscience 353, 209–226. https://doi.org/10.5802/crgeos.62

Aubineau, J., El Abani, A., Bekker, A., Somogyi, A., Bankole, O., Macchiarelli, R., Meunier, A., Riboulleau, A., Reynaud, J.-Y., Konhauser, K.O., El Albani, A., 2019. Microbially induced potassium enrichment in Paleoproterozoic shales and implications for reverse weathering on early Earth. Nature Communications 10, 2370. https://doi.org/10.1038/s41467-019-10620-3

Aubineau, J., El Albani, A., Chi Fru, E., Gingras, M.K., Batonneau, Y., Buatois, L., Geffroy, C., Labanowski, J., Laforest, C., Lemée, L., Mángano, M., Meunier, A., Pierson-Wickmann, A.-C., Recourt, P., Riboulleau, A., Trentesaux, A., Konhauser, K.O., 2018. Unusual microbial mat-related structural diversity 2.1 billion years ago and implications for the Francevillian biota. Geobiology 16, 476–497. https://doi.org/10.1111/gbi.12296

Azziley Azzibrouck, G., 1986. Sedimentologie et geochimie du francevillien b (proterozoique inferieur). Metallogenie des gisements de manganese de moanda, gabon (These de doctorat). Strasbourg 1.

Bankole, O.M., El Albani, A., Meunier, A., Gauthier-Lafaye, F., 2015. Textural and paleo-fluid flow control on diagenesis in the Paleoproterozoic Franceville Basin, South Eastern, Gabon. Precambrian Research 268, 115–134. https://doi.org/10.1016/j.precamres.2015.07.008

Behrensmeyer, A.K., Kidwell, S.M., Gastaldo, R.A., 2000. Taphonomy and Paleobiology. Paleobiology 26, 103–147.

Berner, R.A., 1984. Sedimentary pyrite formation: An update. Geochimica et Cosmochimica Acta 48, 605–615. https://doi.org/10.1016/0016-7037(84)90089-9

Birck, J.L., Barman, M.R., Capmas, F., 1997. Re-Os Isotopic Measurements at the Femtomole Level in Natural Samples - Birck - 1997 - Geostandards Newsletter - Wiley Online Library [WWW Document]. URL https://onlinelibrary.wiley.com/doi/10.1111/j.1751-908X.1997.tb00528.x (accessed 11.4.22).

Briggs, D., 2003. The Role of Decay and Mineralization in the Preservation of Soft-Bodied Fossils. Annual Review of Earth and Planetary Sciences 31, 275–301. https://doi.org/10.1146/annurev.earth.31.100901.144746

737 Briggs, D., Raiswell, R., Bottrell, S., Hatfield, D., Bartels, C., 1996. Controls on the pyritization of
738 exceptionally preserved fossils: an analysis of the Lower Devonian Hunsrück Slate of
739 Germany. American Journal of Science 296, 633–663.
740 Briggs, D.E.G., 1999. Molecular taphonomy of animal and plant cuticles: selective preservation and
741 diagenesis. Philos Trans R Soc Lond B Biol Sci 354, 7–17.
742 https://doi.org/10.1098/rstb.1999.0356
743 Briggs, D.E.G., Kear, A.J., 1993. Decay and Preservation of Polychaetes: Taphonomic Thresholds in
744 Soft-Bodied Organisms. Paleobiology 19, 107–135.
745 Brindley, G.W., Brown, G., 1980. Crystal Structures of Clay Minerals and their X-Ray Identification.
746 https://doi.org/10.1180/mono-5
747 Bros, R., Stille, P., Gauthier-Lafaye, F., Weber, F., Clauer, N., 1992. Sm-Nd isotopic dating of
748 Proterozoic clay material: An example from the Francevillian sedimentary series, Gabon.
749 Earth and Planetary Science Letters 113, 207–218. https://doi.org/10.1016/0012-
750 821X(92)90220-P
751 Butterfield, N.J., 2003. Exceptional Fossil Preservation and the Cambrian Explosion1. Integrative and
752 Comparative Biology 43, 166–177. https://doi.org/10.1093/icb/43.1.166
753 Butterfield, N.J., 1995. Secular distribution of Burgess-Shale-type preservation. Lethaia 28, 1–13.
754 https://doi.org/10.1111/j.1502-3931.1995.tb01587.x
755 Canfield, D.E., Ngombi-Pemba, L., Hammarlund, E.U., Bengtson, S., Chaussidon, M., Gauthier-
756 Lafaye, F., Meunier, A., Riboulleau, A., Rollion-Bard, C., Rouxel, O., Asael, D., Pierson-
757 Wickmann, A.-C., El Albani, A., 2013. Oxygen dynamics in the aftermath of the Great
758 Oxidation of Earth's atmosphere. Proceedings of the National Academy of Sciences 110,
759 16736–16741. https://doi.org/10.1073/pnas.1315570110
760 Conway Morris, S., 1986. The community structure of the Middle Cambrian Phyllopod Bed (Burgess
761 Shale) | The Palaeontological Association [WWW Document]. URL
762 https://www.palass.org/publications/palaeontology-journal/archive/29/3/article_pp423-467
763 (accessed 11.4.22).
764 Creaser, R.A., Papanastassiou, D.A., Wasserburg, G.J., 1991. Negative thermal ion mass spectrometry
765 of osmium, rhenium and iridium. Geochimica et Cosmochimica Acta 55, 397–401.
766 https://doi.org/10.1016/0016-7037(91)90427-7
767 Cuadros, J., Linares, J., 1996. Experimental kinetic study of the smectite-to-illite transformation.
768 Geochimica et Cosmochimica Acta 60, 439–453. https://doi.org/10.1016/0016-
769 7037(95)00407-6
770 El Albani, A., Bengtson, S., Canfield, D.E., Bekker, A., Macchiarelli, R., Mazurier, A., Hammarlund,
771 E.U., Boulvais, P., Dupuy, J.-J., Fontaine, C., Fürsich, F.T., Gauthier-Lafaye, F., Janvier, P.,
772 Javaux, E., Ossa, F.O., Pierson-Wickmann, A.-C., Riboulleau, A., Sardini, P., Vachard, D.,
773 Whitehouse, M., Meunier, A., 2010. Large colonial organisms with coordinated growth in

oxygenated environments 2.1 Gyr ago. Nature 466, 100–104. https://doi.org/10.1038/nature09166

El Albani, A., Bengtson, S., Canfield, D.E., Riboulleau, A., Rollion Bard, C., Macchiarelli, R., Ngombi Pemba, L., Hammarlund, E., Meunier, A., Moubiya Mouele, I., Benzerara, K., Bernard, S., Boulvais, P., Chaussidon, M., Cesari, C., Fontaine, C., Chi-Fru, E., Garcia Ruiz, J.M., Gauthier-Lafaye, F., Mazurier, A., Pierson-Wickmann, A.C., Rouxel, O., Trentesaux, A., Vecoli, M., Versteegh, G.J.M., White, L., Whitehouse, M., Bekker, A., 2014. The 2.1 Ga Old Francevillian Biota: Biogenicity, Taphonomy and Biodiversity. PLoS ONE 9, e99438. https://doi.org/10.1371/journal.pone.0099438

El Albani, A., Mangano, M.G., Buatois, L.A., Bengtson, S., Riboulleau, A., Bekker, A., Konhauser, K., Lyons, T., Rollion-Bard, C., Bankole, O., Lekele Baghekema, S.G., Meunier, A., Trentesaux, A., Mazurier, A., Aubineau, J., Laforest, C., Fontaine, C., Recourt, P., Chi Fru, E., Macchiarelli, R., Reynaud, J.Y., Gauthier-Lafaye, F., Canfield, D.E., 2019a. Organism motility in an oxygenated shallow-marine environment 2.1 billion years ago. Proc Natl Acad Sci U S A 116, 3431–3436. https://doi.org/10.1073/pnas.1815721116

El Albani, A., Mangano, M.G., Buatois, L.A., Bengtson, S., Riboulleau, A., Bekker, A., Konhauser, K., Lyons, T., Rollion-Bard, C., Bankole, O., Lekele Baghekema, S.G., Meunier, A., Trentesaux, A., Mazurier, A., Aubineau, J., Laforest, C., Fontaine, C., Recourt, P., Chi Fru, E., Macchiarelli, R., Reynaud, J.Y., Gauthier-Lafaye, F., Canfield, D.E., 2019b. Organism motility in an oxygenated shallow-marine environment 2.1 billion years ago. Proc Natl Acad Sci USA 116, 3431–3436. https://doi.org/10.1073/pnas.1815721116

A. El Albani, K.O. Konhauser, A. Somogyi, J. Ngwalghoubou Ikouanga, A. Lamboux, J. Blichert-Toft, E. Chi-Fru, C. Fontaine, A. Mazurier, A. Riboulleau, A.-C. Pierson-Wickmann, and F. Albarède, 2023. A search for life in Palaeoproterozoic marine sediments using Zn isotopes and geochemistry. Earth Planetary Sciences Letter (In Press).

Farrell, Ú.C., 2014. Pyritization of Soft Tissues in the Fossil Record: An Overview. The Paleontological Society Papers 20, 35–58. https://doi.org/10.1017/S1089332600002795

Gabbott, S.E., Norry, M.J., Aldridge, R.J., Theron, J.N., 2001. Preservation of fossils in clay minerals; a unique example from the Upper Ordovician Soom Shale, South Africa. Proceedings of the Yorkshire Geological Society 53, 237–244. https://doi.org/10.1144/pygs.53.3.237

Gabbott, S.E., Xian-guang, H., Norry, M.J., Siveter, D.J., 2004. Preservation of Early Cambrian animals of the Chengjiang biota 4.

Gaines, R.R., Droser, M.L., 2010. The paleoredox setting of Burgess Shale-type deposits. Palaeogeography, Palaeoclimatology, Palaeoecology 297, 649–661. https://doi.org/10.1016/j.palaeo.2010.09.014

Gaines, R.R., Hammarlund, E.U., Hou, X., Qi, C., Gabbott, S.E., Zhao, Y., Peng, J., Canfield, D.E., 2012. Mechanism for Burgess Shale-type preservation. Proceedings of the National Academy of Sciences 109, 5180–5184. https://doi.org/10.1073/pnas.1111784109

812 Gaines, R.R., Kennedy, M.J., Droser, M.L., 2005. A new hypothesis for organic preservation of
813 Burgess Shale taxa in the middle Cambrian Wheeler Formation, House Range, Utah.
814 Palaeogeography, Palaeoclimatology, Palaeoecology, Interpretation of Biological and
815 Environmental Changes across the Neoproterozoic-Cambrian Boundary 220, 193–205.
816 https://doi.org/10.1016/j.palaeo.2004.07.034
817 Gauthier-Lafaye, F., 1986. Les gisements d'uranium du Gabon et les réacteurs d'Oklo. Modèle
818 métallogénique de gîtes à fortes teneurs du Protérozoïque inférieur. Sciences Géologiques,
819 bulletins et mémoires 78.
820 Gauthier-Lafaye, F., Weber, F., 1989. The Francevillian (Lower Proterozoic) uranium ore deposits of
821 Gabon. Economic Geology 84, 2267–2285. https://doi.org/10.2113/gsecongeo.84.8.2267
822 Guan, C., Wang, W., Zhou, C., Muscente, A.D., Wan, B., Chen, X., Yuan, X., Chen, Z., Ouyang, Q.,
823 2017. Controls on fossil pyritization: Redox conditions, sedimentary organic matter content,
824 and Chuaria preservation in the Ediacaran Lantian Biota. Palaeogeography,
825 Palaeoclimatology, Palaeoecology, Biosedimentary records of China from the Precambrian to
826 present. 474, 26–35. https://doi.org/10.1016/j.palaeo.2016.05.013
827 Karhu, J., Holland, H., 1996. Carbon isotopes and the rise of atmospheric oxygen. Geology 24.
828 https://doi.org/10.1130/0091-7613(1996)024<0867:CIATRO>2.3.CO;2
829 Knoll, A.H., Whittington, H.B., Morris, S.C., 1985. Exceptional preservation of photosynthetic
830 organisms in silicified carbonates and silicified peats. Philosophical Transactions of the Royal
831 Society of London. B, Biological Sciences 311, 111–122.
832 https://doi.org/10.1098/rstb.1985.0143
833 Lekele Baghekema, S.G., Lepot, K., Riboulleau, A., Fadel, A., Trentesaux, A., El Albani, A., 2017.
834 Nanoscale analysis of preservation of ca. 2.1 Ga old Francevillian microfossils, Gabon.
835 Precambrian Research 301, 1–18. https://doi.org/10.1016/j.precamres.2017.08.024
836 Martin, D., Briggs, D., Parkes, R., 2004. Experimental attachment of sediment particles to invertebrate
837 eggs and the preservation of soft-bodied fossils. Journal of The Geological Society - J GEOL
838 SOC 161, 735–738. https://doi.org/10.1144/0016-764903-164
839 Mayaga-Mikolo, F., 1996. Chronologie des evenements sedimentaires, magmatiques et tectono-
840 metamorphiques du precambrien d'afrique centrale occidentale (gabon) : tectogenese ogooue
841 et heritage archeen (These de doctorat). Clermont-Ferrand 2.
842 Moore, D.M., Reynolds, R.C., 1997. X-ray diffraction and the identification and analysis of clay
843 minerals, 2nd ed. ed. Oxford University Press, Oxford.
844 Muscente, A.D., Hawkins, A.D., Xiao, S., 2015. Fossil preservation through phosphatization and
845 silicification in the Ediacaran Doushantuo Formation (South China): a comparative synthesis.
846 Palaeogeography, Palaeoclimatology, Palaeoecology, Ediacaran Environments and
847 Ecosystems 434, 46–62. https://doi.org/10.1016/j.palaeo.2014.10.013
848 Muscente, A.D., Schiffbauer, J.D., Broce, J., Laflamme, M., O'Donnell, K., Boag, T.H., Meyer, M.,
849 Hawkins, A.D., Huntley, J.W., McNamara, M., MacKenzie, L.A., Stanley, G.D., Hinman,

N.W., Hofmann, M.H., Xiao, S., 2017. Exceptionally preserved fossil assemblages through geologic time and space. Gondwana Research 48, 164–188. https://doi.org/10.1016/j.gr.2017.04.020

Ngombi-Pemba, L., Albani, A.E., Meunier, A., Grauby, O., Gauthier-Lafaye, F., 2014. From detrital heritage to diagenetic transformations, the message of clay minerals contained within shales of the Palaeoproterozoic Francevillian basin (Gabon). Precambrian Research 255, 63–76. https://doi.org/10.1016/j.precamres.2014.09.016

Ngwal'ghoubou Ikouanga J. A. Les interactions argiles-biota paléoprotérozoïque (Gabon) et leurs implications dans la préservation taphonomique. Thèse de doctorat. Université de Poitiers. UFR des sciences fondamentales et appliquées (faculté). 235p

Ossa, F., Pons, M.-L., Bekker, A., Hofmann, A., Poulton, S., Andersen, M., Agangi, A., Gregory, D., Reinke, C., Steinhilber, B., Marin-Carbonne, J., Schoenberg, R., 2023. Zinc enrichment and isotopic fractionation in a marine habitat of the c. 2.1 Ga Francevillian Group: A signature of zinc utilization by eukaryotes? https://doi.org/10.1016/j.epsl.2023.118147

Ossa Ossa, F., El Albani, A., Hofmann, A., Bekker, A., Gauthier-Lafaye, F., Pambo, F., Meunier, A., Fontaine, C., Boulvais, P., Pierson-Wickmann, A.-C., Cavalazzi, B., Macchiarelli, R., 2013. Exceptional preservation of expandable clay minerals in the ca. 2.1Ga black shales of the Francevillian basin, Gabon and its implication for atmospheric oxygen accumulation. Chemical Geology 362, 181–192. https://doi.org/10.1016/j.chemgeo.2013.08.011

Ossa Ossa, F., Hofmann, A., Wille, M., Spangenberg, J.E., Bekker, A., Poulton, S.W., Eickmann, B., Schoenberg, R., 2018. Aerobic iron and manganese cycling in a redox-stratified Mesoarchean epicontinental sea. Earth and Planetary Science Letters 500, 28–40. https://doi.org/10.1016/j.epsl.2018.07.044

Petrovich, R., 2001. Mechanisms of Fossilization of the Soft-Bodied and Lightly Armored Faunas of the Burgess Shale and of Some Other Classical Localities. American Journal of Science 301, 683–726. https://doi.org/10.2475/ajs.301.8.683

Préat, A., Bouton, P., Thiéblemont, D., Prian, J.-P., Ndounze, S.S., Delpomdor, F., 2011. Paleoproterozoic high δ13C dolomites from the Lastoursville and Franceville basins (SE Gabon): Stratigraphic and synsedimentary subsidence implications. Precambrian Research 189, 212–228. https://doi.org/10.1016/j.precamres.2011.05.013

Reynaud, J.-Y., Trentesaux, A., El Albani, A., Aubineau, J., Ngombi-Pemba, L., Guiyeligou, G., Bouton, P., Gauthier-Lafaye, F., Weber, F., 2018. Depositional setting of the 2·1 Ga Francevillian macrobiota (Gabon): Rapid mud settling in a shallow basin swept by high-density sand flows. Sedimentology 65, 670–701. https://doi.org/10.1111/sed.12398

Rhoads, D., Epstein, W., 2003. Osmotic control ofkdp operon expression in Escherichia coli (potassium transport / lac fusion / turgor pressure | Semantic Scholar [WWW Document]. URL https://www.semanticscholar.org/paper/Osmotic-control-ofkdp-operon-expression-in-coli-

%28-%2F-Rhoads-Epstein/abbf75eb6c4081904997d6a057b597a991a72604 (accessed 11.4.22).

Santiago Ramos, D.P., Morgan, L.E., Lloyd, N.S., Higgins, J.A., 2018. Reverse weathering in marine sediments and the geochemical cycle of potassium in seawater: Insights from the K isotopic composition (41K/39K) of deep-sea pore-fluids. Geochimica et Cosmochimica Acta, Chemistry of oceans past and present: A Special Issue in tribute to Harry Elderfield 236, 99–120. https://doi.org/10.1016/j.gca.2018.02.035

Selby, D., Creaser, R., 2004. Macroscale NTIMS and microscale LA-MC-ICP-MS Re-Os isotopic analysis of molybdenite: Testing spatial restrictions for reliable Re-Os age determinations, and implications for the decoupling of Re and Os within molybdenite. Geochimica et Cosmochimica Acta 68, 3897–3908. https://doi.org/10.1016/j.gca.2004.03.022

Selby, D., Creaser, R., 2003. Re-Os geochronology of organic rich sediments: An evaluation of organic matter analysis methods. Chemical Geology 200, 225–240. https://doi.org/10.1016/S0009-2541(03)00199-2

Stankiewicz, B.A., Briggs, D.E.G., Michels, R., Collinson, M.E., Flannery, M.B., Evershed, R.P., 2000. Alternative origin of aliphatic polymer in kerogen. Geology 28, 559–562. https://doi.org/10.1130/0091-7613(2000)28<559:AOOAPI>2.0.CO;2

Stautz, J., Hellmich, Y., Fuss, M.F., Silberberg, J.M., Devlin, J.R., Stockbridge, R.B., Hänelt, I., 2021. Molecular Mechanisms for Bacterial Potassium Homeostasis. J Mol Biol 433, 166968. https://doi.org/10.1016/j.jmb.2021.166968

Sun, H., Chen, M., Zou, L., Shu, R., Ruan, R., 2015. Study of the kinetics of pyrite oxidation under controlled redox potential. Hydrometallurgy 155, 13–19. https://doi.org/10.1016/j.hydromet.2015.04.003

Tegelaar, E.W., de Leeuw, J.W., Derenne, S., Largeau, C., 1989. A reappraisal of kerogen formation. Geochimica et Cosmochimica Acta 53, 3103–3106. https://doi.org/10.1016/0016-7037(89)90191-9

Thiéblemont, D., Bouton, P., Préat, A., Goujou, J.-C., Tegyey, M., Weber, F., Ebang Obiang, M., Joron, J.L., Treuil, M., 2014. Transition from alkaline to calc-alkaline volcanism during evolution of the Paleoproterozoic Francevillian basin of eastern Gabon (Western Central Africa). Journal of African Earth Sciences 99, 215–227. https://doi.org/10.1016/j.jafrearsci.2013.12.007

Thiéblemont, D., Castaing, C., Billa, M., Bouton, P., Préat, A., 2009. NOTICE EXPLICATIVE DE LA CARTE GÉOLOGIQUE ET DES RESSOURCES MINÉRALES DE LA RÉPUBLIQUE GABONAISE À 1/1 000 000 384.

Völkening, J., Walczyk, T., G. Heumann, K., 1991. Osmium isotope ratio determinations by negative thermal ionization mass spectrometry. International Journal of Mass Spectrometry and Ion Processes 105, 147–159. https://doi.org/10.1016/0168-1176(91)80077-Z

924 Weber, F., 1968a. Une série précambrienne du Gabon : le Francevillien. Sédimentologie, géochimie,
925 relations avec les gites minéraux associés. Sciences Géologiques, bulletins et mémoires 28.
926 Weber, F., 1968b. SÉDIMENTOLOGIE, GÉOCHIMIE, RELATIONS AVEC LES GITES
927 MINÉRAUX ASSOCIÉS 331.
928 Wilson, L.A., Butterfield, N.J., 2014. Sediment Effects on the Preservation of Burgess Shale-Type
929 Compression Fossils. PALAIOS 29, 145–153.
930
931